Renewable Energy 111 (2017) 227–244

Contents lists available at ScienceDirect

Renewable Energy

journal homepage: www.elsevier.com/locate/renene

Characterizing and analyzing ramping events in wind power, solar power, load, and netload

Mingjian Cui [a], Jie Zhang [a, *], Cong Feng [a], Anthony R. Florita [b], Yuanzhang Sun [c], Bri-Mathias Hodge [b]

[a] Department of Mechanical Engineering, University of Texas at Dallas, Richardson, TX 75080, USA
[b] National Renewable Energy Laboratory, Golden, CO 80401, USA
[c] School of Electrical Engineering, Wuhan University, Wuhan 430072, China

ARTICLE INFO

Article history:
Received 8 May 2016
Received in revised form
3 February 2017
Accepted 2 April 2017
Available online 7 April 2017

Keywords:
Dynamic programming
Load
Netload
Optimized swinging door algorithm
Solar power
Wind power

ABSTRACT

One of the biggest concerns associated with integrating a large amount of renewable energy into the power grid is the ability to handle large ramps in the renewable power output. For the sake of system reliability and economics, it is essential for power system operators to better understand the ramping features of renewables, load, and netload. In this paper, an optimized swinging door algorithm (OpSDA) is adopted and extended to accurately and efficiently detect ramping events. For wind power ramps detection, a process of merging "bumps" (that have a different changing direction) into adjacent ramping segments is integrated to improve the performance of the OpSDA method. For solar ramps detection, ramping events that occur in both clear-sky and measured (or forecasted) solar power are removed to account for the diurnal pattern of solar generation. Ramping features are extracted and extensively compared between load and netload under different renewable penetration levels (i.e., 9.77%, 15.85%, and 51.38%). Comparison results show that: (i) netload ramp events with shorter durations and smaller magnitudes occur more frequently when renewable penetration level increases, and the total number of ramping events also increases; and (ii) different ramping characteristics are observed in load and netload even at a low renewable penetration level.

1. Introduction

Renewable energy, especially wind and solar energy, has become a focus in government policies, power and energy industries, and academic research [1–3]. However, the uncertainty and variability in wind and solar energy present new challenges to the power system that aims to retain secure, reliable, and economic operations at high renewable penetrations. Among many challenges, severe fluctuation incidents with large magnitudes and short durations, so-called "ramping events", are a major concern of power system operators [4,5].

Ramping events occur in wind power generation, solar power generation, load, and also netload, and are caused by a number of different factors. For wind power ramping events (WPREs), they are usually caused by complicated physical processes and atmospheric phenomena, such as thunderstorms, wind gusts, cyclones, and low-level jets [6]. For solar power ramping events (SPREs), the short-term microclimates (e.g., passing clouds) are the main reason beyond diurnal variability. When a transient cloud passes over photovoltaic (PV) panels, the inverter output will ramp down quickly [7]. Load ramp events (LREs) are mainly driven by human behavior [8], and building heating and cooling or large industrial loads are largely affected by weather. Netload is the total electric demand in the system minus wind and solar. Understanding the ramping features in netload becomes more critical with increasing renewable penetrations. Electric load is relatively more stable compared to renewable energy sources. However, under certain circumstances, up-ramping load with down-ramping renewable energy sources (or down-ramping load with up-ramping renewable energy sources) can create more severe netload ramping events. To better understand the relationship between renewable and load ramps, it is helpful to compare the ramping characteristics in both load and netload with different renewable penetration levels. Ramping events are generally parameterized by the following features: ramping start/end, ramping duration, ramping rate, and ramping magnitude.

* Corresponding author.
E-mail address: jiezhang@utdallas.edu (J. Zhang).

http://dx.doi.org/10.1016/j.renene.2017.04.005
0960-1481/

Nomenclature

NRE	netload ramp event
LRE	load ramp event
SPRE	solar power ramp event
WPRE	wind power ramp event
sYeY	start-YES-end-YES event
sYeN	start-YES-end-NO event
sNeY	start-NO-end-YES event
sNeN	start-NO-end-NO event
POD	probability of detection
CSI	critical success index
FBS	frequency bias score
SR	success ratio
DT	time resolution of sampling data

1.1. Research motivation and contribution

It is known that the level of uncertainty and variability in power systems tends to increase with additional renewable energy. However, the quantified impacts of renewable energy on the power system ramping characteristics are still unclear to the power system operators. To better understand the impacts of renewable penetration and load ramps, it is very important to study the ramping characteristics in both load and netload.

Ramping events in netload present different variability characteristics under different renewable penetration levels, which has been posed and discussed by power system operators and academic researchers [9–13]. However, many of these questions have not yet been addressed. For example, by what magnitude will netload ramping events increase? How will ramping durations, magnitudes, and rates change due to the renewables increase?

Moreover, power system operators usually need to solve scheduling issues at different time resolutions. For example, the economic dispatch (ED) is normally processed at a shorter time resolution (e.g., 15 min or 5 min); whereas unit commitment (UC) is generally processed at a longer time resolution (often hourly time resolution for planning on the order of days). Thus, it is also important to quantify and analyze ramping events that occur at different time resolutions. However, there are few research papers that do the aforementioned work.

The contributions of this paper are: (i) developing a ramping event detection model to compare and analyze ramping features at multiple renewable penetration levels and different time resolutions; (ii) developing a suite of metrics with a contingency table and a performance diagram to evaluate the ramps detection performance; (iii) intuitively comparing and analyzing the impacts of increasing renewable penetration levels on both the load and netload; and (iv) comparing the difference of probability distributions of ramping features between wind and solar ramping events.

The remainder of this paper is organized as follows: the specific ramping definitions are presented in Section 2. The OpSDA based ramp detection methods for WPREs, SPREs, LREs, and NREs are provided in Section 3. A suite of metrics to evaluate the performance of ramps detection are discussed in Section 4. Section 5 presents the statistical analysis results of a case study for a utility company in the northwestern United States. Conclusions and a discussion of future work are given in Section 6.

1.2. Overview of wind power ramp events

The research on WPREs can be generally classified into three directions: WPREs detection, WPREs forecasting, and WPREs application. The WPREs detection uses a mathematical algorithm and wind power ramping definitions to extract all the wind power ramps from actual or forecasted wind power data. The WPREs detection methods can be directly applied to historical measured wind power data to extract all historical ramping events. Statistical and machine learning methods can then be developed based on the historical ramping events to directly forecast WPREs. The accuracy of WPREs forecasting highly depends on the accuracy of WPREs detection.

Regarding WPREs detection, Sevlian et al. [14,15] proposed an optimal detection technique to identify all WPREs by defining a family of scoring functions associated with any ramping rules and using recursive dynamic programming. Zhang et al. [16] adopted the swinging door algorithm (SDA) to extract ramp events from actual and forecasted wind power time series. Cui et al. [17] developed an optimized swinging door algorithm (OpSDA) to improve ramp detection performance, by segregating wind power time series with the SDA and merging all ramps with a dynamic programming algorithm. Kamath [18,19] used feature selection techniques from data mining to determine ramps in wind power generation.

Regarding WPREs forecasting, Cui et al. [20,21] modeled the wind power generation as a stochastic process by using a neural network and a genetic algorithm, then forecasted the probability distributions of three WPREs properties. Cutler et al. [22] compared the efficiency of the Wind Power Prediction Tool (WPPT) and the Mesoscale Limited Area Prediction System (MesoLAPS) for WPREs forecasting. Zareipour et al. [23] mined historical data and predicted the class of WPREs using support vector machines. Greaves et al. [24] quantified the temporal uncertainty to provide an indication of the likely timing of WPREs.

Detected and forecasted WPREs can be used in power system operations. Kubik et al. [25] examined the strategies that could be taken to respond to wind ramping challenges through improving existing thermal plants flexibility. Porter et al. [26] proposed multiple approaches to handle wind ramping by holding available system resources and multiple control area cooperating actions, such as sharing reserves or energy imbalances. One case of WPREs in the wind plant of Qiaowan (Gansu, China) is shown in Fig. 1 with a 15-min time resolution. Here we define a WPRE as the change in total wind power that is greater than 20% of the wind capacity. As shown in Fig. 1, there are four up-ramps (in red lines) and four down-ramps (in green lines).

1.3. Overview of solar ramp events

Solar ramp events can be classified into two categories based on the studied subjects: solar irradiance ramp events and solar power

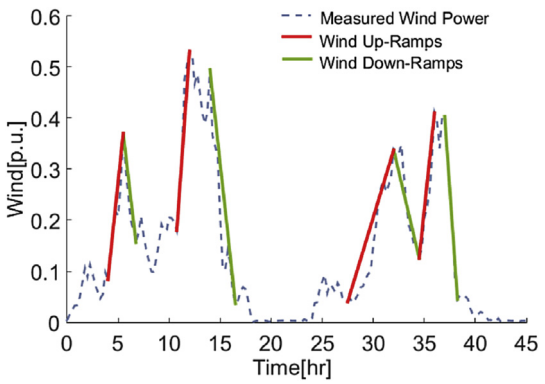

Fig. 1. The case of WPREs for a wind plant in Qiaowan, China with a 15-min time resolution.

ramp events. The study of solar irradiance ramp events is essential for inverter control, solar plant management, and real-time dispatch operations for solar power plants. The study of solar power ramp events helps the balancing authorities better understand and manage these ramp events, and sometimes even utilize these natural power ramps in regulation reserves, load-following reserves, and sub-hourly economic dispatch.

Several studies on solar irradiance ramp events can be found in the literature. Chu et al. [27] integrated cloud tracking techniques and artificial neural network algorithms to predict one minute averaged solar irradiance ramps, showing that the proposed forecasting platform outperformed the persistence model. Hansen et al. [28] utilized the distribution of solar irradiance ramp events as one of metrics to evaluate the consistency of observed irradiance data. Reno and Stein [29] studied measured solar irradiance ramping rates based on hourly cloud classified satellite images. Willy et al. [30] compared different methods of computing solar irradiance ramp events with ramping frequency, duration, and magnitude.

Regarding solar power ramp events (SPREs), Hill et al. [31] utilized battery energy storage systems to mitigate solar power ramp rate and frequency issues. Arias-Castro et al. [32] studied the spatial correlations of solar power ramp rates by modeling cloud fields using a spatial Poisson process. Hummon et al. [33] analyzed solar power ramping in the state of Gujarat in India using high-resolution solar data and found that the total magnitude of solar power ramping went up with increased solar capacity. Hodge et al. [34] analyzed solar ramp distributions at different timescales and weather patterns. Florita et al. [35] applied the swinging door algorithm to identify both solar and wind ramping events from historic operational data, and indicated that defining novel metrics and informing various power system models are critical tasks for the identification of SPREs. Cui et al. [36] proposed an optimized ramping detection method to identify SPREs.

One case of SPREs for a utility company in the northwestern United States is shown in Fig. 2 with a 15-min time resolution. Here we define an SPRE as a change in total solar power that is greater than 20% of the solar capacity after removing ramps that also occur in clear-sky power. As shown in Fig. 2, there is one up-ramp (the red line) and one down-ramp (the green line). SPREs mainly occur during mid-days when the solar generation is near the peak output.

1.4. Overview of load and netload ramping events

Wind and solar power are often regarded as a type of negative load. Therefore, the netload (P_{NL}) is defined as the load demand (P_L) minus the renewable energy sources from wind power (P_W) and solar power (P_S), given by:

$$P_{NL} = P_L - P_W - P_S \tag{1}$$

Most of the work in the literature mainly focuses on how to handle netload ramp events using traditional generators (e.g., thermal units) in power system dispatching. Wu et al. [9] modeled flexible up/down ramping capability of thermal units to respond to hourly netload, finding that flexible ramping reduced renewable energy curtailments. Xu and Tretheway [10] designed up and down flexible ramping products to address operational challenges to maintain power balance in the real-time dispatch. Navid et al. [11] suggested that the existing generators of all types maximize the availability of their operational netload-following ramp flexibility, and also suggested to introduce new flexible ramp sources such as demand response. Wang et al. [12] assumed that the flexible ramping product market aims to manage the increasing netload ramp events, and found that flexible ramping products can enhance market efficiency. Ela et al. [13] proposed that an up- and down-ramp product market can be established with renewable energy and demand load to cope with netload ramp events. One case of netload ramp events (NREs) for a utility company in the northwestern United States is shown in Fig. 3 at a 15-min time resolution. Here we define an NRE as the change in total netload that is greater than 5% of the maximum netload value. As shown in Fig. 3, there are eight up-ramps and six down-ramps.

2. Characterizing ramping events

The definition of a ramp event generally depends on the specific application at different utilities and independent system operators (ISOs). Kamath [18] defined a ramp event if the deviation between the start and end of an interval was larger than a predefined threshold value, and suggested that this definition could neglect the ramp events occurring in the middle of an interval. Kamath [19] also defined a ramp event if the deviation between the maximum and minimum values of an interval was larger than a threshold value without considering how the signal decreased or increased. Zheng et al. [37] defined a ramp event based on the absolute magnitude difference of the deviation (between the start and end of an interval) and the time interval length. Ramp events occurring in the middle of an interval were also neglected. In this study, ramps in wind power, solar power, load, and netload are defined as follows.

2.1. Definitions of wind and solar power ramp events

We use four WPREs definitions that were originally defined in Ref. [38], which also apply to SPREs in this paper. Note that the

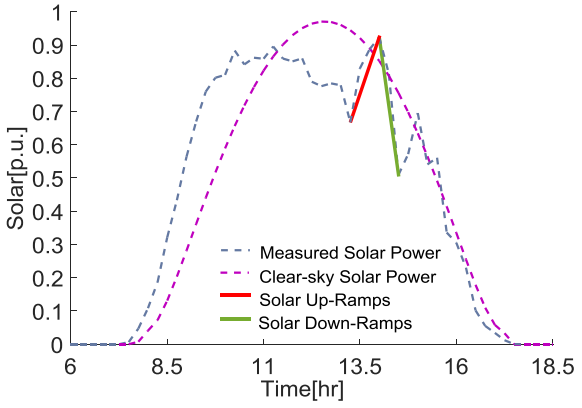

Fig. 2. The case of SPREs of a utility company in the northwestern United States with a 15-min time resolution.

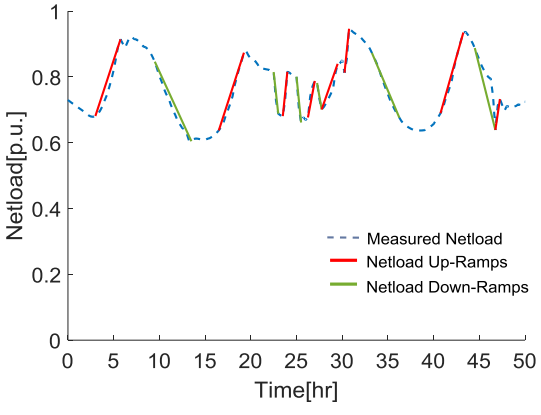

Fig. 3. The case of NREs of a utility company in the northwestern United States with a 15-min time resolution.

ramping change rate is the ratio of ramping magnitude to ramping duration, given by:

$$Change\ Rate = \frac{Ramping\ Magnitude}{Ramping\ Duration}$$

- Ramp Definition 1: the change in wind (or solar) power output that is greater than 20% of the installed wind (or solar) capacity;
- Ramp Definition 2: the change in wind (or solar) power output that is greater than 20% of the installed wind (or solar) capacity within a time span of 4 h or less;
- Ramp Definition 3: the change rate in wind (or solar) power output that is greater than 3% of the installed wind (solar) capacity; and
- Ramp Definition 4: an up-ramp is defined as the change in wind (or solar) power output that is greater than 20% of the installed wind (or solar) capacity within a time span of 4 h or less; a down-ramp is defined as the change in wind (or solar) power output that is greater than 15% of the installed wind (solar) power capacity within a time span of 4 h or less.

For power system operations, down-ramps are generally more challenging to manage than up-ramps. This is because upward wind (or solar) power ramps can be managed by other means, such as adjusting other generators' schedules, or wind (or solar) curtailment if necessary. However, when downward wind (or solar) power ramps occur, power system operators have to compensate the deficit of wind (or solar) power by increasing other generating capacities. Thus, a lower difference threshold (15%) is chosen for down-ramps, and a higher difference threshold (20%) is used to define up-ramps in Definition 4. Because of the diurnal pattern of solar power, ramps occurring in both measured solar power and clear-sky solar power are not true SPREs, as they are expected to occur. The diurnal up-ramping (from sunrise to noon) or down-ramping (from noon to sunset) tendency should not be considered as a ramp event. Thus, we also need to identify these “fake ramp events”.

2.2. Definitions of load and netload ramp events

Since the load and netload signal are relatively stable compared to wind and solar power, we define load and netload ramp events with smaller threshold values than those of WPREs and SPREs, as shown in Table 1.

- Ramp Definition 1: the change in total load (or netload) that is greater than 5% of the maximum load (or netload) value;
- Ramp Definition 2: the change in total load (or netload) that is greater than 5% of the maximum load (or netload) value within a time span of 4 h or less;
- Ramp Definition 3: the change rate in total load (or netload) that is greater than 3% of the maximum load (or netload) value; and
- Ramp Definition 4: an up-ramp is defined as the change in total load (or netload) that is greater than 5% of the maximum load (or netload) value within a time span of 4 h or less; a down-ramp is defined as the change in total load (or netload) that is greater than 7% of the maximum load (or netload) value within a time span of 4 h or less.

3. Methodology for detecting ramp events

A recently developed ramp detection method, the optimized swinging door algorithm (OpSDA), is adopted and extended in this paper [17], [36]. The OpSDA is a two-stage process method. The first stage is a data segregation process based on the swinging door algorithm (SDA) [39]. SDA is used to segregate power signals (e.g., wind power, solar power, load, and netload) according to the user-specified definition of a ramp. The second stage is an optimization process based on a dynamic programming algorithm. Dynamic programming is used to merge adjacent segments that are segregated with the same ramp changing direction in the first stage. The details of the OpSDA method can be found in Ref. [17]. A data-driven platform for detecting ramp events is developed in this paper, as shown in Fig. 4, which consists of three main components: Database, Detection, and Diagnosis. The Detection part is similar to some signal decompensation methods. Renewable energy and load data are collected from utilities and ISOs. This platform can be used to compare and analyze the ramp event features and provide informative suggestions for power system operations.

3.1. Swinging door algorithm (SDA)

SDA is a data compression algorithm that was originally proposed by Bristol [39], which has been widely used in many areas. Recently SDA has been gradually applied in the renewable energy community [40], [41]. Fig. 5 illustrates the SDA method for identifying ramps in the power signal. A power value is compressed if a straight line drawn (between the last stored power value and the next power value) does not cause any intermediate point to fall outside the area partitioned by the up and down segment bounds; otherwise, a power value is kept and the last power value is set as the start of the next coming compression interval. As shown in Fig. 5, Point B falls within the area ABC (Segment 1) and therefore is compressed; whereas, Point C falls outside the area ABCD and makes the compression process of the area ABC (Segment 1) terminate at Point C. Then the next segment (Segment 2) starts from Point C. Likewise, segments 2, 3, and 4 are generated. After compression, Points B, D, F, H, and I are all compressed. The only tunable parameter in SDA is the compression deviation, which is defined as the ‘swinging door width’, $\pm\varepsilon$.

When SDA is used to detect ramp events, modification and improvements need to be applied to this method. As shown in Fig. 5, the aforementioned Segment 1 and Segment 2 are two adjacent segments segregated by SDA. Assuming that both segments comply with ramping definitions, SDA would identify these two segments as two separate up-ramp events. However, it should be only one up-ramp in the area ABCDE from the visual inspection. This indicates that after the SDA segregation, adjacent segments could be further combined or merged to optimize the SDA detection results.

In the second stage, since wind power, solar power, load, and netload have different characteristics based on their own physical attributes, dynamic programming will be applied in different ways. Specifically, due to the relatively stable attribute of load and netload, we directly use dynamic programming to optimize the segments obtained in the first stage. Regarding the solar power, ramps simultaneously occurring in both clear-sky and actual solar power generation should be removed. Regarding the wind power, due to high fluctuations in wind power, dynamic programming usually breaks off when some small ramping intervals appear with very small durations and magnitudes. Under this circumstance, these small intervals should be merged into adjacent ramping events in the dynamic programming process. Therefore, we propose three types of OpSDA-based methods to detect wind power, solar power, load, and netload ramp events, as discussed in the following sections.

Table 1
Four ramp definitions in wind power, solar power, netload, and load.

		Definition 1	Definition 2	Definition 3	Definition 4
WPRE	Up-ramp	≥20%	≥20%	–	≥20%
	Down-ramp	≥20%	≥20%	–	≥15%
	Time span	≤ +∞	≤4 h	≤ +∞	≤4 h
	Ramp rate	–	–	≥3%	–
SPRE	Up-ramp	≥20%	≥20%	–	≥20%
	Down-ramp	≥20%	≥20%	–	≥15%
	Time span	≤ +∞	≤4 h	≤ +∞	≤4 h
	Ramp rate	–	–	≥3%	–
NRE/LRE	Up-ramp	≥5%	≥5%	–	≥5%
	Down-ramp	≥5%	≥5%	–	≥7%
	Time span	≤ +∞	≤4 h	≤ +∞	≤4 h
	Ramp rate	–	–	≥3%	–

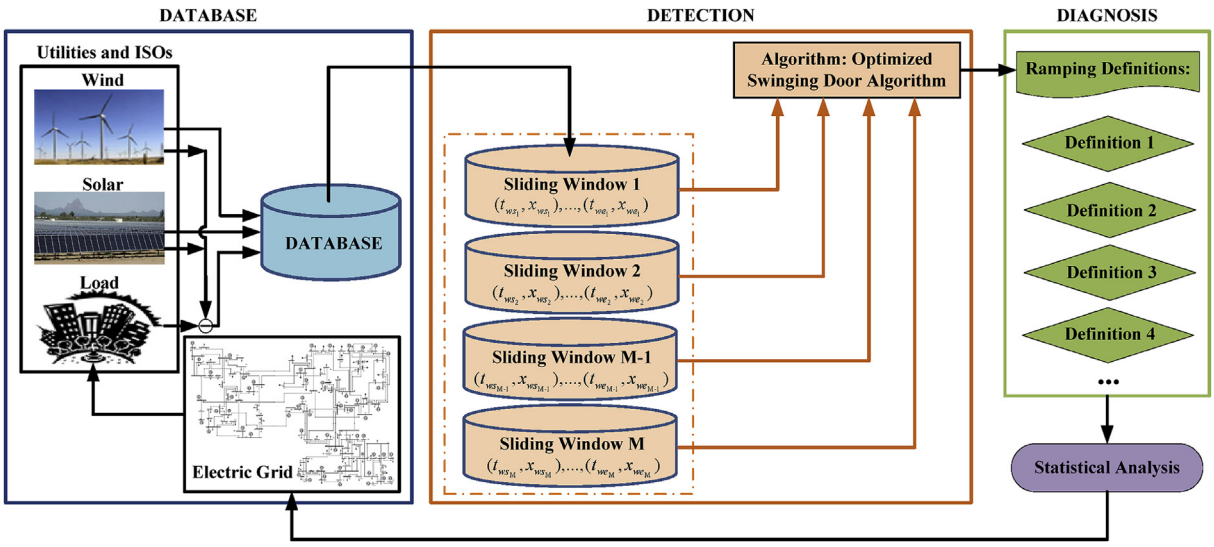

Fig. 4. A data-driven platform for detecting ramp events.

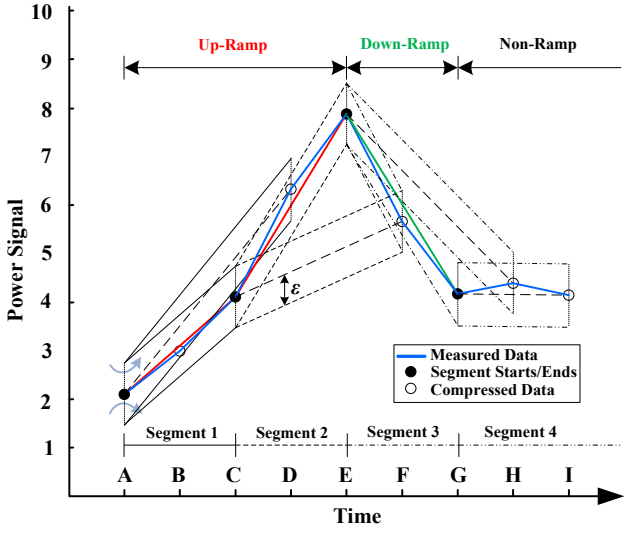

Fig. 5. The SDA for detecting ramps in power.

3.2. OpSDA based load and netload ramp event (LRE and NRE) detection

As for NREs detection, we directly utilize a dynamic programming algorithm to optimize the segments generated by SDA. Dynamic programming is a method to solve a complex problem by breaking it down into a collection of simpler sub-problems. It is applicable to problems exhibiting the properties of overlapping subproblems and optimal substructures. Dynamic programming has been widely used in the literature to solve a variety of engineering problems [42], [43].

The objective of the ramp detection is to maximize the length score function, which corresponds to a load or netload ramp event. In this study, an increasing length score function, S, is designed based on the length of the segments segregated by the SDA. Given a load or netload signal interval, (i, j), of all discrete time points and an objective function, J, of the dynamic programming model, an LRE or NRE is detected by maximizing the objective function:

$$J(i,j) = \max_{i<k\le j}[S(i,k) + J(k,j)], \quad i<j \tag{2}$$

s.t.

$$S(i,j) > S(i,k) + S(k+1,j), \quad \forall i<k<j \tag{3}$$

$$S(i,j) = (j-i)^2 \times R(i,j) \tag{4}$$

where $J(i, j)$ can be computed as the maximum over $(i–j)$ subproblems. The term of $S(i, k)$ is a positive score value corresponding to the interval, (i, k), which conforms to a super-additivity property in Eq. (3). There is a family of score functions satisfying Eq. (2), and the score function presented in Ref. [14] is adopted in

this paper, expressed as Eq. (4). The term of $R(i, j)$ represents a ramp within the time interval, (i, j), which has been introduced in Section 2 and extensively used in the literature [44]. If $R(i, j)$ conforms to the threshold of ramp definitions, $R(i, j)$ is assigned to be 1; otherwise, $R(i, j)$ is assigned to be 0.

Based on Eqs. (2)–(4), the optimization process can proceed inductively as follows. Assuming that the number of NREs is M ($\forall m$: $1 \le m < M$), the NRE interval set, $\xi = \{E_m, \ldots, E_M\}$, is the set of intervals, E_m=(s_m, e_m), where s_m represents the start of segment E_m and e_m represents the end of segment E_m; and the non-NRE interval set, $\overline{\xi} = \{\overline{E_m}, \ldots, \overline{E_M}\}$, is the set of intervals, $\overline{E_m} = (\overline{s_m}, \overline{e_m})$. If $\forall(\overline{s_m}, \overline{e_m}) \in \overline{\xi}$ and $\forall i, j$: $\overline{s_m} < i < j < \overline{e_m}$, then:

$$\begin{aligned} &R(i,j) = 0 \\ &S(i,j) = 0 \\ &J(\overline{s}_m, \overline{e}_m) = 0 \end{aligned} \tag{5}$$

If $\forall\ (s_m, e_m) \in \xi$ and $\forall i, j$: $s_m < i < j < e_m$, the objective function $J(s_m, e_m)$ is expressed as:

$$\begin{aligned} J(s_m, e_m) &= \max_{s_m < k_1 < e_m} [S(s_m, k_1) + J(k_1 + 1, e_m)] \\ &= \max_{s_m < k_1 < e_m} S(s_m, k_1) + \max_{k_1+1 < k_2 < e_m} [S(k_1 + 1, k_2) + J(k_2 + 1, e_m)] \\ &= \max_{s_m < k_1 < k_2 < \cdots < e_m} S(s_m, k_1) + S(k_1 + 1, k_2) \end{aligned} \tag{6}$$

Thus, considering Eq. (2), $J(s_m, e_m)$ is $J(s_m, e_m) = S(s_m, e_m)$. An optimal event sequence of NREs (or LREs) and non-NREs (or non-LREs) can be presented as $\Theta = \{E_m, \overline{E_m}, E_{m+1}, \overline{E_{m+1}}, \ldots, E_M, \overline{E_M}\}$ and $\{\overline{E_m}, E_{m+1}, \overline{E_{m+1}}, \ldots, E_M, \overline{E_M}\}$, respectively, for a given L load or netload signal series. It is assumed that p_{s_m} is the power value at the start of segment E_m, and $p_{\overline{e_M}}$ is the power value at the end of segment $\overline{E_M}$. If a load or netload signal series $p_{s_m}, \ldots, p_{\overline{e_M}}$ with the event sequence $\Theta = \{E_m, \overline{E_m}, E_{m+1}, \overline{E_{m+1}}, \ldots, E_M, \overline{E_M}\}$ has a solution to Eq. (2) being $J(s_m, \overline{e_M})$, the solution is shown in Eqs. (7) and (9). If a load or netload signal series $p_{\overline{s_m}}, \ldots, p_{\overline{e_M}}$ with the event sequence $\Theta = \{\overline{E_m}, E_{m+1}, \overline{E_{m+1}}, \ldots, E_M, \overline{E_M}\}$ has a solution to Eq. (2) being $J(\overline{s_m}, \overline{e_M})$, the solution is shown in Eqs. (8) and (10):

Thus, considering Eq. (3), $J(s_m, \overline{e_M})$ in Eq. (7) can be transformed to:

$$J\left(s_m, \overline{e_M}\right) = S(s_m, e_m) + J\left(\overline{s_m}, \overline{e_M}\right) \tag{9}$$

Likewise, considering Eq. (4), $J(\overline{s_m}, \overline{e_M})$ in Eq. (8) is:

$$\begin{aligned} J\left(\overline{s_m}, \overline{e_M}\right) &= \max_{\overline{s_m} < k_1 < k_2 < \cdots < k_{i-1} < k_i \le \overline{e_m}} J\left(k_i + 1, \overline{e_M}\right) \\ &= J\left(s_{m+1}, \overline{e_M}\right) \end{aligned} \tag{10}$$

If a load or netload signal series is $p_{s_1}, \ldots, p_{\overline{e_M}}$, the solution is:

$$J\left(s_1, \overline{e_M}\right) = \sum_{m=1}^{M} S(s_m, e_m) \tag{11}$$

If a load or netload signal series is $p_{\overline{s_1}}, \ldots, p_{\overline{e_M}}$, the solution is:

$$J\left(\overline{s_1}, \overline{e_M}\right) = \sum_{m=2}^{M} S(s_m, e_m) \tag{12}$$

Fig. 6 shows M sliding windows with the start point and the end point. A set of load or netload ramps E_i will be detected in each window. The number of load or netload ramps in each window may be different. In brief, all the load or netload segments are first segregated by SDA with a predefined compression deviation ε. Then all extracted load or netload segments are input into the second stage (the red block in Fig. 6) and merged to yield a set of optimized load or netload ramp events.

3.3. OpSDA based solar power ramp event (SPRE) detection

As for SPREs detection, Eq. (4) in Section 3.2 is modified based on [15] by using a new variable, $C(i, j)$, which represents the rule of a clear-sky solar ramp event. This ramping definition $C(i, j)$ is applied to remove all clear-sky solar ramp events from all ramp events in the measured or forecasted solar power generation. The score function is updated as: $S(i, j)$=$(j-i)^2 \times [1-C(i, j)]$. If there is a clear-sky solar ramp event, $C(i, j)$ equals 1 and then $S(i, j)$ equals 0. The clear-sky solar ramp event is removed. If there is not a clear-sky

$$\begin{aligned} J\left(s_m, \overline{e_M}\right) &= \max_{s_m < k_1 \le e_m} \left[S(s_m, k_1) + J\left(k_1 + 1, \overline{e_M}\right)\right] \\ &= \max_{s_m < k_1 \le e_m} \left\{S(s_m, k_1) + \max_{k_1+1 < k_2 \le e_m} \left[S(k_1 + 1, k_2) + J\left(k_2 + 1, \overline{e_M}\right)\right]\right\} \\ &= \max_{s_m < k_1 \le e_m} \left\{S(s_m, k_1) + \max_{k_1+1 < k_2 \le e_m} \left\{S(k_1 + 1, k_2) + \cdots + \max_{k_{i-1}+1 < k_i \le e_m} \left[S(k_{i-1}, k_i) + J\left(k_i + 1, \overline{e_M}\right)\right]\right\}\right\} \\ &= \max_{s_m < k_1 < k_2 < \cdots < k_{i-1} < k_i \le e_m} \{S(s_m, k_1) + S(k_1 + 1, k_2) + \cdots + S(k_{i-1}, k_i)\} + \max_{k_{i-1}+1 < k_i \le e_m} J\left(k_i + 1, \overline{e_M}\right) \end{aligned} \tag{7}$$

$$\begin{aligned} J\left(\overline{s_m}, \overline{e_M}\right) &= \max_{\overline{s_m} < k_1 \le \overline{e_m}} \left[S\left(\overline{s_m}, k_1\right) + J\left(k_1 + 1, \overline{e_M}\right)\right] \\ &= \max_{\overline{s_m} < k_1 \le \overline{e_m}} \left\{S\left(\overline{s_m}, k_1\right) + \max_{k_1+1 < k_2 \le \overline{e_m}} \left[S(k_1 + 1, k_2) + J\left(k_2 + 1, \overline{e_M}\right)\right]\right\} \\ &= \max_{\overline{s_m} < k_1 \le \overline{e_m}} \left\{S\left(\overline{s_m}, k_1\right) + \max_{k_1+1 < k_2 \le \overline{e_m}} \left\{S(k_1 + 1, k_2) + \cdots + \max_{k_{i-1}+1 < k_i \le \overline{e_m}} \left[S(k_{i-1}, k_i) + J\left(k_i + 1, \overline{e_M}\right)\right]\right\}\right\} \\ &= \max_{\overline{s_m} < k_1 < k_2 < \cdots < k_{i-1} < k_i \le \overline{e_m}} \left\{S\left(\overline{s_m}, k_1\right) + S(k_1 + 1, k_2) + \cdots + S(k_{i-1}, k_i)\right\} + \max_{k_{i-1}+1 < k_i \le \overline{e_m}} J\left(k_i + 1, \overline{e_M}\right) \end{aligned} \tag{8}$$

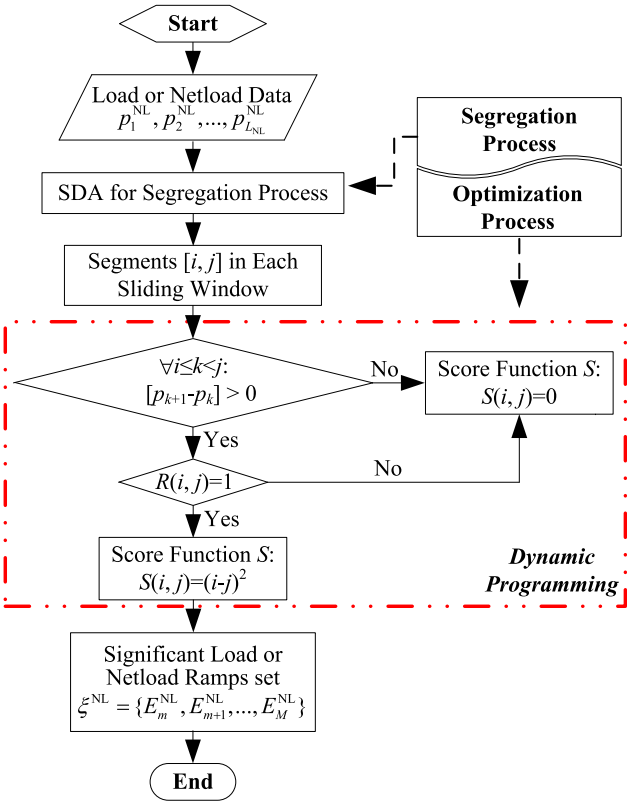

Fig. 6. Overall framework of detecting LREs and NREs.

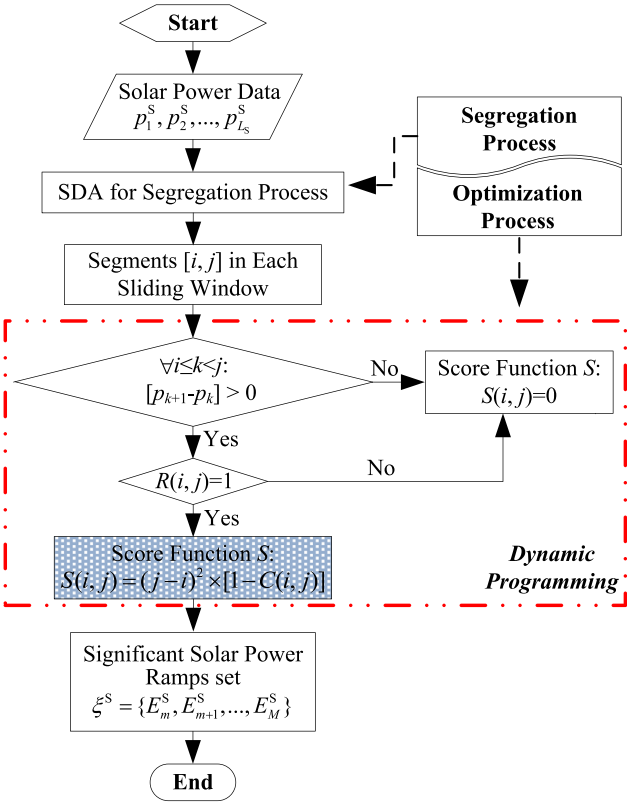

Fig. 7. Overall framework of detecting SPREs.

solar ramp event, $C(i, j)$ equals 0 and then $S(i, j)$ equals 1. The dynamic programming continues to maximize the score function to detect an accurate SPRE. Except for the equality constraint $C(i, j)$ in Eq. (4), the SPRE detection method shares the same variables and constraints with the LRE/NRE detection method. The term of $R(i, j)$ represents a ramp within the time interval, (i, j), in measured or forecasted solar power. In this paper, we use four definitions of ramp events that were defined in Section 2 to determine both $R(i, j)$ and $C(i, j)$. All the solar power segments are first segregated by SDA with a predefined compression deviation ε in Section 3.1. Then all extracted solar power segments are input into the second stage (the red block in Fig. 7) and merged to yield a set of optimized SPREs.

3.4. OpSDA based wind power ramp event (WPRE) detection

As for WPREs detection, one of the interesting findings in a previous paper [17] was the presence of small ramps, classified as non-WPREs, which are termed "bumps" in this paper and set as $B(i, j)$ in the formulations below. In this study, one bump is defined as a small non-WPRE that occurs in a very short time duration with a small magnitude. The changing direction of a bump (e.g., a down-bump between two up-ramps, or an up-bump between two down-ramps) makes the iteration of the dynamic programming break off abruptly due to the strict super-additivity property in Eq. (3). When a bump occurs, it breaks one integrated WPRE into two discrete ramps, which affects the performance of WPREs detection. To address this issue, the second stage of the dynamic programming optimization is improved so that it can also merge ramps and bumps with different changing directions. If $B(i, j)$ conforms to the threshold of bump definitions, $B(i, j)$ is assigned to be 1; otherwise, $B(i, j)$ is assigned to be 0. During the recursion, bumps are also considered and merged into the WPREs. The overall flowchart of detecting WPREs is shown in Fig. 8. The score function in Eq. (4) is improved to consider bump events, given by:

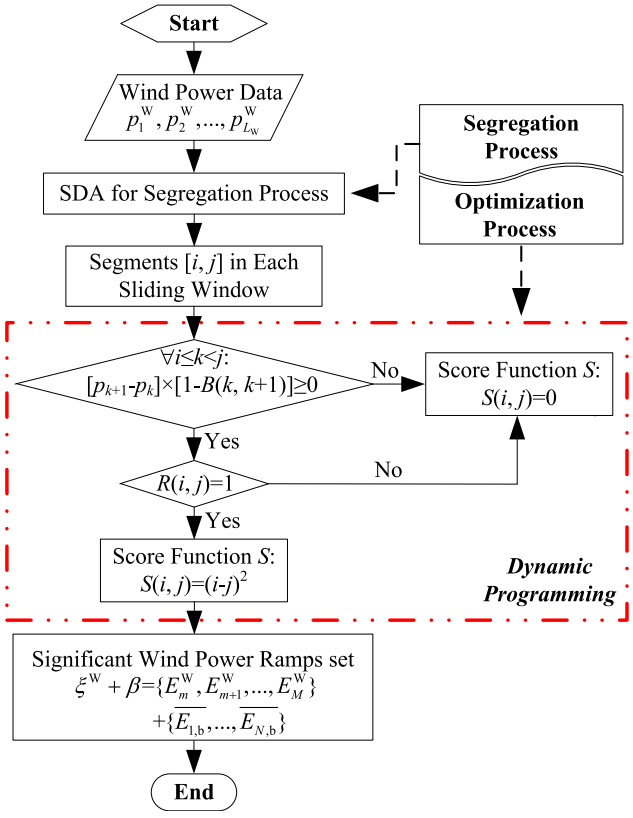

Fig. 8. Overall framework of detecting WPREs.

$$[p_{k+1} - p_k] \times [1 - B(k, k+1)] \geq 0, \quad \forall i \leq k < j \tag{13}$$

Within a bump interval set $\beta = \{\overline{E_{1,b}}, \ldots, \overline{E_{n,b}}, \ldots, \overline{E_{N,b}}\}$, the members $\overline{E_{n,b}} = (\overline{s_{n,b}}, \overline{e_{n,b}})$ are constructed from the nth non-WPRE interval, $\overline{E_n}$, where $\forall(s_n, e_n)$, $(s_n + 1, e_n + 1) \in \xi$: $1 \leq s_n, e_{n+1} < L$ and $(\overline{s_{n,b}}, \overline{e_{n,b}}) = (e_n + 1, s_{n+1} - 1)$. Then a wind power series with the bump can be represented as $\Theta = \{\ldots, E_n, \overline{E_{n,b}}, E_{n+1}, \ldots, E_M, \overline{E_M}\}$. The solution is compressed after combining the two WPREs, E_n and E_{n+1}, around one bump, $\overline{E_{n,b}}$, in Eq. (14).

$$(s_n, e_n + 1) \rightarrow (s_n, e_n) \tag{14}$$

4. Metrics to evaluate the ramp detection performance

It is critically important for power system operators to be aware when a ramping event starts (ramping start) and terminates (ramping end). This ramping information could be used in a variety of power system applications, such as unit commitment (especially in stochastic unit commitment problems), flexible ramping reserve determination [45], and other scheduling problems to reduce the costs caused by ramping events [46], [47]. Thus, the accuracy of detecting the ramping start and end is an important metric to evaluate a ramping detection method. To this end, we propose a metric to estimate the detection performance of LREs, NREs, SPREs, and WPREs at different time resolutions. The proposed metric focuses on the detection accuracy of the ramp start and end points. Specific descriptions are given next.

Fig. 9(a) and (c) show that an accurate ramp, denoted as YES, is extracted when the start (or end) of a ramping event is a maximum (or minimum) point. Under this circumstance, the segment $[p(i), p(i + DT)]$ has an opposite direction to the segment $[p(i-DT), p(i)]$, where DT represents the time resolution of sampling data. A mathematical relationship is expressed as:

$$\frac{p(i+DT) - p(i)}{p(i) - p(i-DT)} < 0, \ \mathrm{DT} \in \{1-, 5-, 15-, \text{and } 60-\text{minute}\} \ \text{(YES)} \tag{15}$$

Conversely, an inaccurate ramp, denoted as NO, is extracted when the start (or end) of a ramping event is not an actual ramping "start" (or "end"), as shown in Fig. 9(b) and (d). The end of the up-ramp in Fig. 9(b) should be the next point $(i + DT)$ rather than the current point (i) and the start of this up-ramp should be the last point $(i\text{-}DT)$ rather than the current point (i), which makes the detected result inaccurate; likewise in Fig. 9(d). Hence, we define the mathematical relationship as:

$$\frac{p(i+DT) - p(i)}{p(i) - p(i-DT)} > 0, \ \mathrm{DT} \in \{1-, 5-, 15-, \text{and } 60-\text{minute}\} \ \text{(NO)} \tag{16}$$

To evaluate the ramping detection results in load, netload, solar, and wind, we use a contingency table and a performance diagram for quantitative and visual analysis. All detection results are grouped into four categories based on whether the OpSDA method extracts the actual ramps or not. In Table 2, *sYeY* (start-YES-end-YES event) represents the number of ramps with both the ramping start and end points accurately identified; *sYeN* (start-YES-end-NO event) represents the number of ramps with only ramping start points accurately identified; *sNeY* (start-NO-end-YES event) represents the number of ramps with only ramping end points accurately identified; *sNeN* (start-NO-end-NO event) represents the number of ramps with both the ramping start and end points NOT accurately identified; and *N* is total number of ramping events.

Based on the contingency table, a suite of metrics are derived for ramping detection performance evaluation. *Probability of detection* (POD) is defined as the ratio between the number of start-YES-end-YES ramping events (*sYeY*) and the number of all end-YES ramping events ($sYeY + sNeY$), which indicates the fraction of start-YES-end-YES points that are accurately identified in all end-YES events.

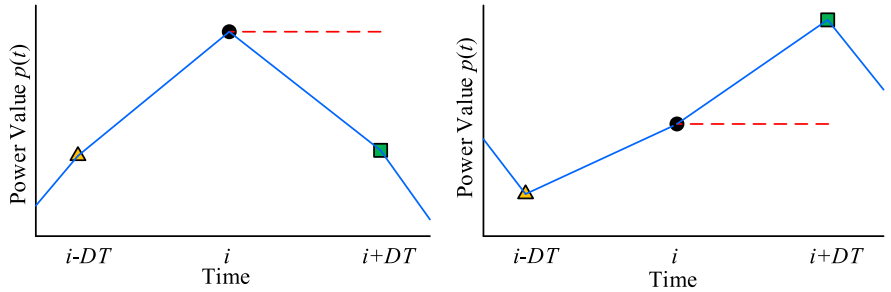

(a) Accurately detected (YES) the end of an up-ramp or the start of a down-ramp

(b) Inaccurately detected (NO) the start or the end of an up-ramp

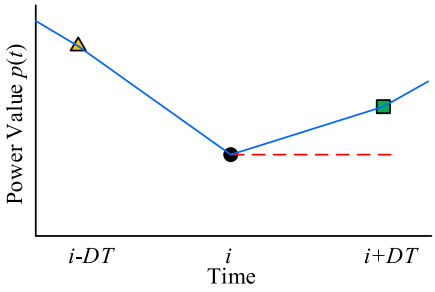

(c) Accurately detected (YES) the start of an up-ramp or the end of a down-ramp

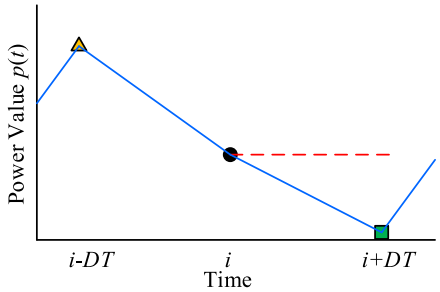

(d) Inaccurately detected (NO) the start or the end of a down-ramp

Fig. 9. Four possible scenarios for ramping detection.

Table 2
Contingency table for ramps detection.

	End (YES)	End (NO)	Total
Start (YES)	*sYeY* (*hits*)	*sYeN* (*start hits only*)	$sYeY + sYeN$
Start (NO)	*sNeY* (*end hits only*)	*sNeN* (*misses*)	$sNeY + sNeN$
Total	$sYeY + sNeY$	$sYeN + sNeN$	$N = sYeY + sYeN + sNeY + sNeN$

$$\mathrm{POD} = \frac{sYeY}{sYeY + sNeY} \tag{17}$$

Critical success index (CSI) represents the ratio between the number of start-YES-end-YES (*sYeY*) ramping events and the number of all start-YES and all end-YES ramping events ($sYeY + sNeY + sYeN$), given by:

$$\mathrm{CSI} = \frac{sYeY}{sYeY + sNeY + sYeN} \tag{18}$$

The value of CSI is between 0 and 1, with 1 representing perfect detection and 0 representing the worst detection. The CSI takes into account all the detected YES ramping events (including only start-YES, only end-YES, and start-YES-end-YES events).

Frequency bias score (FBS) measures the ratio between the number of all start-YES ramping events ($sYeY + sYeN$) and the number of all end-YES ramping events ($sYeY + sNeY$), given by:

$$\mathrm{FBS} = \frac{sYeY + sYeN}{sYeY + sNeY} \tag{19}$$

if FBS is less than 1, it means that more ramping end points are correctly extracted than ramping start points; otherwise, more ramping start points are correctly extracted.

Success ratio (SR) measures the ratio between the number of start-YES-end-YES ramping events (*sYeY*) and the number of all start-YES ramping events ($sYeY + sYeN$), given by:

$$\mathrm{SR} = \frac{sYeY}{sYeY + sYeN} \tag{20}$$

where SR indicates the fraction of start-YES-end-YES ramping events that are accurately identified in all start-YES events.

The specific relationship among the POD, CSI, FBS, and SR can be visualized on a performance diagram [48] as below:

$$\mathrm{CSI} = \frac{1}{\frac{1}{\mathrm{POD}} + \frac{1}{\mathrm{SR}} - 1} \tag{21}$$

$$\mathrm{FBS} = \frac{\mathrm{POD}}{1 - \mathrm{FAR}} = \frac{\mathrm{POD}}{\mathrm{SR}} \tag{22}$$

5. Results

5.1. Sites selection and data summary

In this section we analyze the time series of measured wind power, solar power, and load data from a utility company in the northwestern United States. Each dataset of wind, solar, and load contains 7,884,012 samples representing measured data sampled every 4 s. Clear-sky solar power generation is calculated and converted from irradiance to power using the PV_LIB toolbox [49]. These wind power, solar power, and load data span from October 1, 2012 to September 30, 2013. The total wind energy produced over the year is 381,732 MWh; the total solar energy produced is 228,634 MWh; and the total load is 11,201,067 MWh. Therefore, the penetration level of renewable energy is approximately 5.45%. To study the monthly ramping events, we use the monthly maximum value of wind power (solar power, load, or netload) as the benchmark capacity, as listed in Table 3.

As for power system operations and electricity markets design, it is important to understand how the penetration of renewable energy affects the characteristics of conventional load ramp events, especially with high renewable penetrations. Thus, we extensively compare the ramping features (magnitude and duration) between the load and netload, including: (i) a 5.45% penetration level of renewable energy with the measured data; and (ii) three scenarios with 9.77%, 15.85%, and 51.38% renewable penetrations derived from a scaling method.

A method is developed to scale up the renewable penetration level based on the measured data with the 5.45% penetration. Different scaling strategies are applied to wind and solar power. As for solar penetrations, considering the diurnal pattern, we directly multiply the baseline solar power data by 2 (or 3) based on the solar power smoothing characteristics shown in Ref. [50]. Due to the higher variability characteristics of wind power resulting from the disparate geographical locations and wake effects, a sophisticated scaling strategy is developed for wind power. The original utility wind power data, $\mathbf{P}_{\mathrm{UWP}}$, is scaled up based on the open source data, $\mathbf{P}_{\mathrm{NREL}}$, simulated by the Wind Integration National Dataset (WIND) Toolkit produced by the National Renewable Energy Laboratory (NREL) [51]. This method aims to simulate the variability propagation during the scaling process, by taking the following steps.

1) The data of a simulated wind farm located nearest to the utility company are chosen as the baseline wind power data. Then the data of another N-1 simulated wind farms close to the utility company are set as the scaled wind power data. The scaling factor of NREL WIND Toolkit data, $\lambda^{\mathrm{N}}_{\mathrm{NREL},t}$, is calculated as:

$$\lambda^{\mathrm{N}}_{\mathrm{NREL},t} = \frac{\sum_{n=1}^{\mathrm{N}} p^{n}_{\mathrm{NREL},t}}{p^{1}_{\mathrm{NREL},t}} \tag{23}$$

2) Assume that the scaling factor of the measured wind power at the utility, $\lambda^{\mathrm{N}}_{\mathrm{UWP},t}$, is approximately equal to that of WIND Toolkit data, given by:

$$\lambda^{\mathrm{N}}_{\mathrm{UWP},t} \approx \lambda^{\mathrm{N}}_{\mathrm{NREL},t} \tag{24}$$

3) The scaled wind power data for the utility at time t is formulated as:

$$p^{\mathrm{N}}_{\mathrm{UWP},t} = \lambda^{\mathrm{N}}_{\mathrm{UWP},t} \times p_{\mathrm{UWP},t} \tag{25}$$

where $t = 1, 2, \ldots, \mathrm{T}$ and T is the length of wind power data; $\mathbf{P}_{\mathrm{UWP}}$ represents the actual time series and $p_{\mathrm{UWP},t} \in \mathbf{P}_{\mathrm{UWP}}$; and $\mathbf{P}^{\mathrm{N}}_{\mathrm{UWP}}$ represents the scaled time series and $p^{\mathrm{N}}_{\mathrm{UWP},t} \in \mathbf{P}^{\mathrm{N}}_{\mathrm{UWP}}$.

The actual wind power data of the studied location is doubled when $\mathrm{N} = 2$, and the renewable penetration is 9.77%. Likewise, the actual wind power data is tripled when $\mathrm{N} = 3$, and the renewable penetration is 15.85%. Corresponding wind farm locations selected

Table 3
Benchmark capacity of measured load, solar power, wind power, and netload.

Month	Wind Power (MW)	Solar Power (MW)	Load (MW)	Netload (MW)
10/2012	126	59	2295	1645
11/2012	117	76	1488	1469
12/2012	120	68	1658	1645
01/2013	121	75	1656	1657
02/2013	120	89	1569	1531
03/2013	122	96	1406	1398
04/2013	127	97	1829	1737
05/2013	123	94	2053	1901
06/2013	127	96	2846	2715
07/2013	127	96	3019	2902
08/2013	125	96	2819	2680
09/2013	127	92	2596	2446

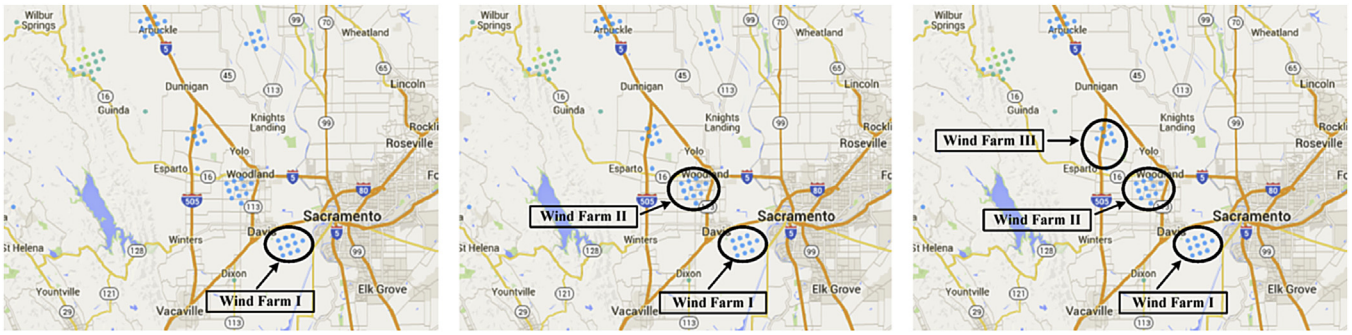

(a) Base wind penetration scenario (N=1) (b) Doubled wind penetration scenario (N=2) (c) Tripled wind penetration scenario (N=3)

Fig. 10. Locations of the three selected wind farms near the utility company.

Table 4
Contingency table values for ramps detection of Definition 1 with four time resolutions.

Variable	Metric	1-h		15-min		5-min		1-min	
		End (YES)	End (NO)	End (YES)	End (NO)	End (YES)	End (NO)	End (YES)	End (NO)
Wind	Start (YES)	133	259	182	252	405	276	555	155
	Start (NO)	298	634	302	618	347	273	174	169
Solar	Start (YES)	100	154	330	121	224	74	153	39
	Start (NO)	189	384	120	183	57	148	26	135
Netload	Start (YES)	99	103	63	101	79	86	88	86
	Start (NO)	93	101	98	136	90	145	93	144

from the WIND Toolkit are shown in Fig. 10.

5.2. Accuracy evaluation of the OpSDA detection method

In this section, we use the estimation metrics with the performance diagram proposed in Section 4 to analyze the detection effectiveness in wind power, solar power, and netload at different time resolutions. Table 4 lists the contingency table values for ramps detection of Definition 1 with four time resolutions of wind, solar, and netload.

For the performance diagram in Fig. 11, (i) the bottom axis represents SR, indicating the fraction of start-YES-end-YES events that are accurately identified in all start-YES events; (ii) the left axis represents POD, indicating the fraction of start-YES-end-YES points that are accurately identified in all end-YES events; (iii) the diagonal dashed lines represent FBS with the specific values on the right and top axes, indicating which type (start or end) of ramping points is detected more accurately; (iv) the dashed curves represent CSI with the specific values on the right-inside graph border. The closer the results to the top-right corner are, the better OpSDA performs.

Fig. 11 compares ramping detection performance at multiple time resolutions with four different ramping definitions in wind power, solar power, and netload. The four analyzed time resolutions are: 1-, 5-, 15-, and 60-min. It is observed from Fig. 11 that SPREs detection has larger SR, POD, and CSI values than NREs and WPREs detection at both the 5- and 15-min time resolutions, indicating that SPREs are more accurately detected at these two time resolutions. For WPREs, the detection results (square points) move towards the top right corner of the performance diagrams with increasing time resolutions, showing that the 1-h time resolution detection has the largest metrics values. This is because the intra-hour variability is mitigated by averaging the wind power from 4-s to the 1-h time resolution. For NREs, although NREs detection at the 1-min time resolution in Definition 2 has the smallest metrics values, the detection results are more concentrated around the center of the performance diagrams for other definitions and time resolutions due to the smaller variability of netload. Another interesting finding is the tendency that all the FBS values are approximately distributed around 1, indicating that the method performs equally well for ramping start and end points detection.

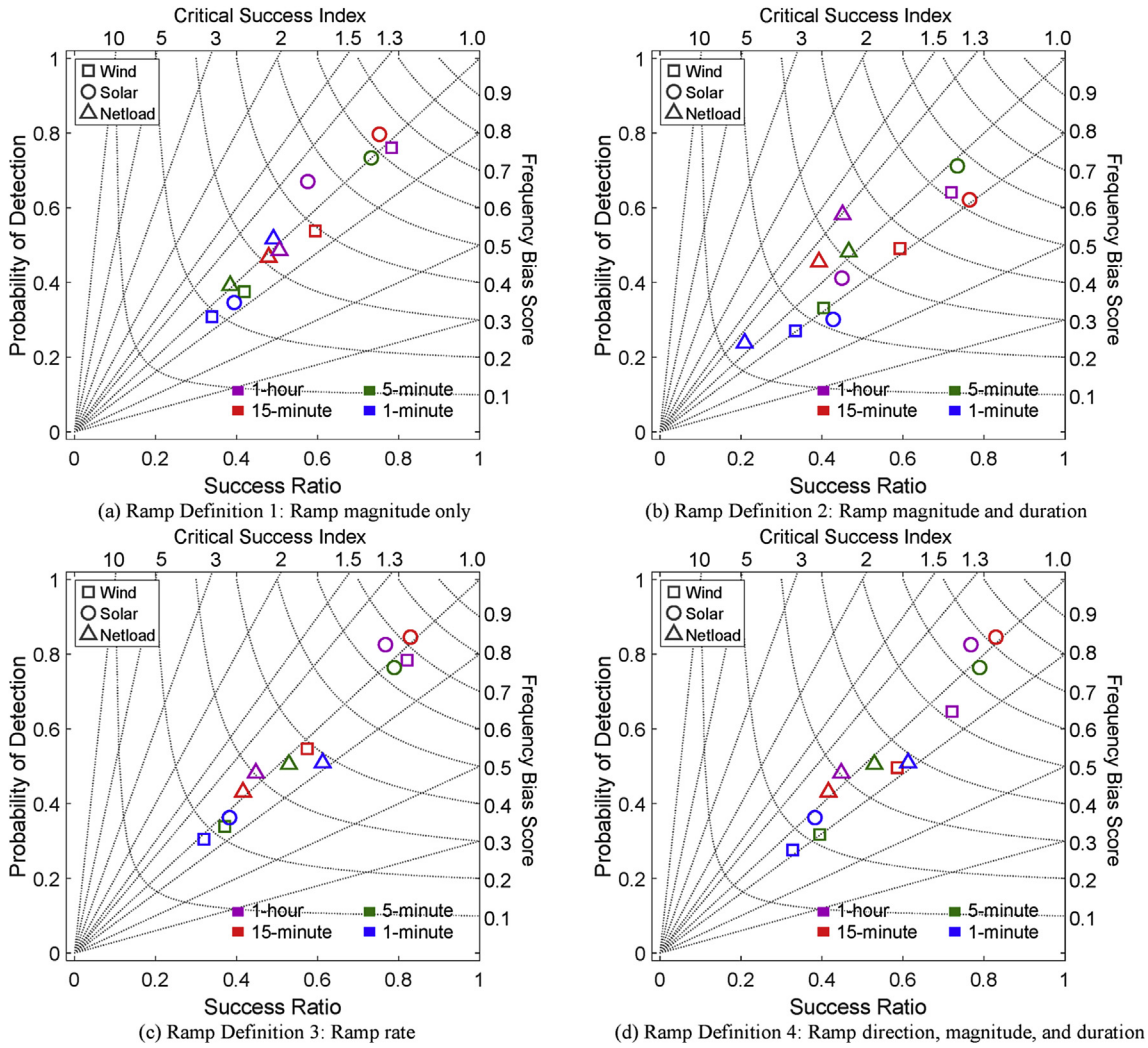

Fig. 11. Comparison of OpSDA detection performance in wind power, solar power, and netload at four time resolutions and four ramping definitions.

5.3. Comparison of LREs and NREs

In this section, we compare the difference between LREs and NREs at three renewable penetration levels (i.e., 9.77%, 15.85%, and 51.38%) by separating the up- and down-ramps in a scatter diagram. We also analyze and compare the three ramping features (ramping duration, magnitude, and rate) at the 5- and 60-min time resolutions between the load and netload with a 9.77% renewable penetration. Based on the simulation results, the impacts of renewable energy on load are visually shown in this section.

5.3.1. Comparison of LREs and NREs with different renewable penetration levels

For LREs in Fig. 12(a) or 12(b), there are one up-ramp cluster and one down-ramp cluster. LRE up-ramps at the 15-min time resolution spread more than those at the 1-h time resolution. With the integration of renewable energy into load, the up-ramp cluster in LREs is more tightly distributed than that in NREs as shown in Figs. 12(c) and 11(d), indicating that up-ramp durations become more variable in NREs. For LREs at the 1-h time resolution, most up-ramp magnitudes concentrate around 0.2 p.u., whereas for NREs most up-ramp magnitudes concentrate between 0.2 p.u. and 0.6 p.u.

When the penetration level increases to 9.77% in Fig. 12(c) and (d), the aggregated data center starts to disperse for both up- and down-ramps. Finally when the penetration increases to 51.38% in Fig. 12(g) and (h), the concentration on the right-y-axis completely disappears and more sparse up-ramps present as well as down-ramps. There are more ramps with shorter durations and smaller magnitudes occurring at the 51.38% penetration level due to the highly increasing renewable variability. Comparing the left four subfigures to the right four in Fig. 12, the subhourly (15-min time resolution) variability makes this phenomenon more distinct than that of the hourly data at 60-min time resolution. Moreover, the number of ramping events also increases with increasing the renewable penetration level, as shown in Table 5. This observation would help power system operators to make better plans to manage ramp events with high renewable penetrations, such as utilizing the ramping events information (e.g., ramping product market design) in system operations, or mitigate ramping events (e.g., ramping control based on energy storage system) for the power balance.

5.3.2. Comparison of ramping duration

Fig. 13 compares the probability density distributions of ramping duration in load and netload. LREs and NREs have almost the same distributions in Definitions 2 and 4, whereas the peak duration of LREs is larger than that of NREs in Definition 1 due to the

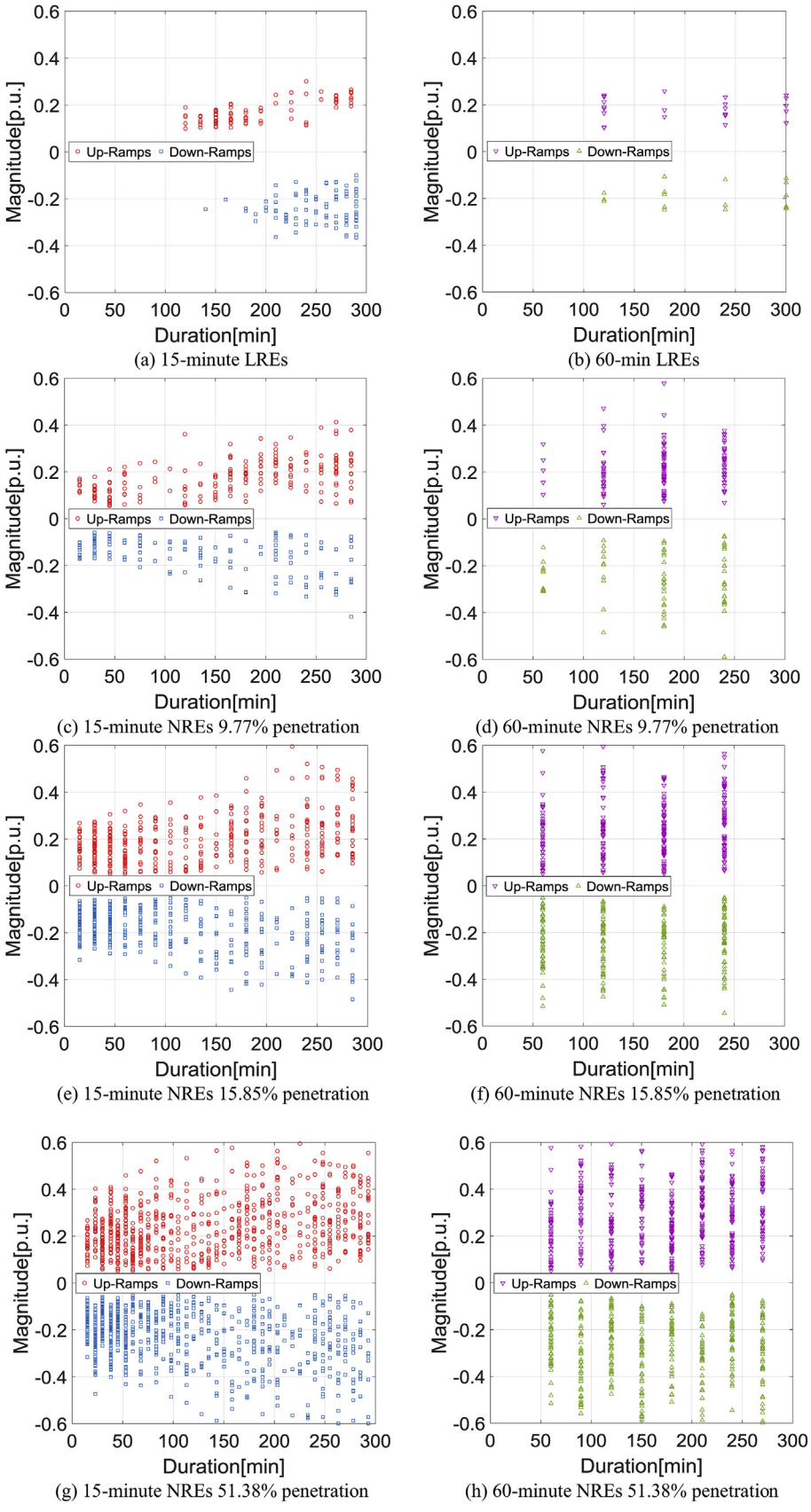

Fig. 12. Scatter diagrams of up- and down-ramps under different renewable penetrations.

Table 5
Number of ramps under different penetrations of renewable energy.

Time Resolution	LREs	NREs with Different Renewable Penetrations		
	0	9.77%	15.85%	51.38%
15-min	269	578	619	1,128
60-min	112	499	569	1,055

integration of renewables. For NREs, the 5- and 60-min time resolutions have almost the same distributions in Definitions 1 and 3. It means that the ramping duration of NREs is stable between different time resolutions. For Definitions 1, 2, and 4, when the time resolution changes from 5-min to 60-min, the peak value of the distribution for LREs decreases and the tails become wider and heavier.

5.3.3. Comparison of ramping magnitude

Fig. 14 compares the probability density distributions of ramping magnitude in load and netload. LREs have sharper peaks than NREs in Definitions 1, 2, and 4. It means more LREs with smaller magnitudes occur with a greater probability. For LREs, distributions of magnitude at 5- and 60-min time resolutions are only similar with Definition 4 and show substantial differences with Definitions 2 and 3. For NREs, distributions of magnitude are very similar for all the four definitions at both 5- and 60-min time resolutions with a slight fluctuation in Definitions 2 and 4.

5.3.4. Comparison of ramping rate

Fig. 15 compares the probability density distributions of ramping rate in load and netload. The distributions of LREs are generally shifted to the right compared to the distributions of NREs in Definitions 2, 3, and 4. It means that netload ramping rates will increase due to the renewable integration. For NREs, distributions of ramping rate are relatively similar between 5- and 60-min time resolutions with Definitions 1 and 3, which presents a similar trend as that of ramping duration and magnitude.

5.4. Comparison of WPRE and SPRE features

In this section, we analyze and compare the three ramping features (ramping duration, magnitude, and rate) at the 5- and 60-min time resolutions in wind and solar. Probability density functions of ramping duration, magnitude, and rate are calculated by the kernel smoothing function estimate in MATLB R2015a [52].

5.4.1. Comparison of ramping duration

Fig. 16 compares the probability density distributions of ramping duration between wind power and solar power. For WPREs in Definitions 1 and 3, when the time resolution changes from 5-min to 60-min, the peak value of the distribution decreases and the tails become heavier. For WPREs in Definitions 2 and 4, the peak probability density is consistent when increasing the ramp duration from the 5-min time resolution to the 60-min time resolution. To cope with WPREs, power system operators need to provide ramping reserves for a longer time in the UC model (at the 60-min time resolution) than in the ED model (at the 5-min time resolution).

For SPREs in Definitions 1 to 4, when the time resolution changes from 5-min to 60-min, the peak value of the distribution decreases and the tails become heavier. The peak ramping duration is longer at the 60-min time resolution than at the 5-min time resolution. To cope with SPREs, power system operators also need to provide ramping reserves for a longer time in the UC model (at the 60-min time resolution) than in the ED model (at the 5-min time resolution).

At the 5-min time resolution (dash lines), the probability densities of WPREs are lower with a smaller peak value and heavier tails than those of SPREs. The peak ramping duration of WPREs is longer than that of SPREs. Power system operators need to provide ramping reserves for a longer time to cope with WPREs than SPREs in the ED model (at the 5-min time resolution). At the 60-min time resolution (solid lines), the peak ramping duration of WPREs is

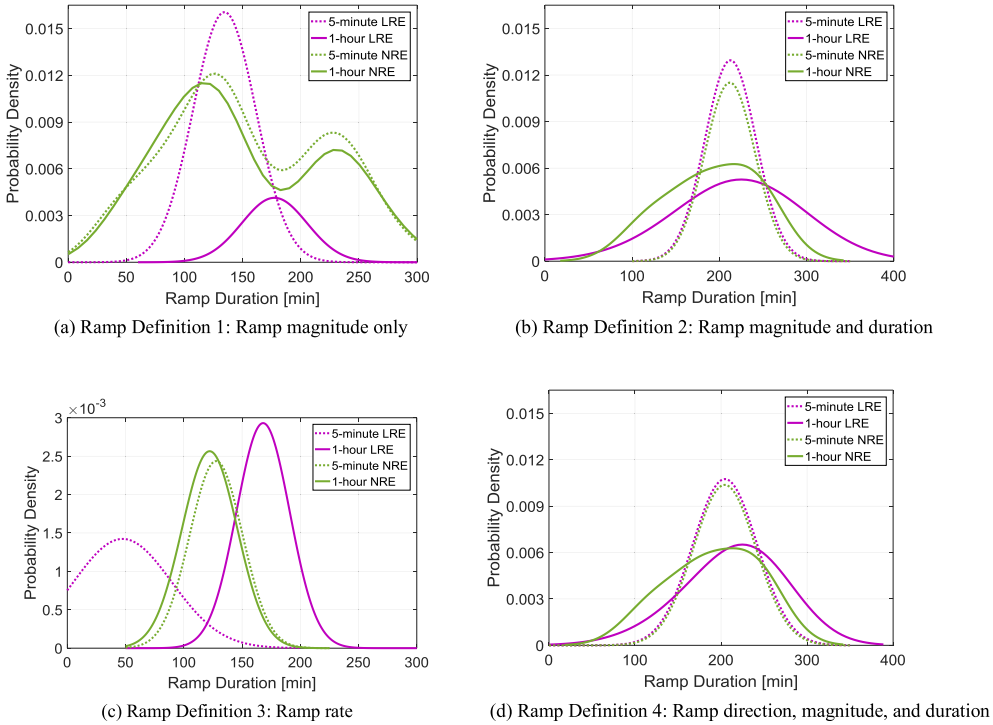

(a) Ramp Definition 1: Ramp magnitude only

(b) Ramp Definition 2: Ramp magnitude and duration

(c) Ramp Definition 3: Ramp rate

(d) Ramp Definition 4: Ramp direction, magnitude, and duration

Fig. 13. Comparison of ramping duration in load and netload.

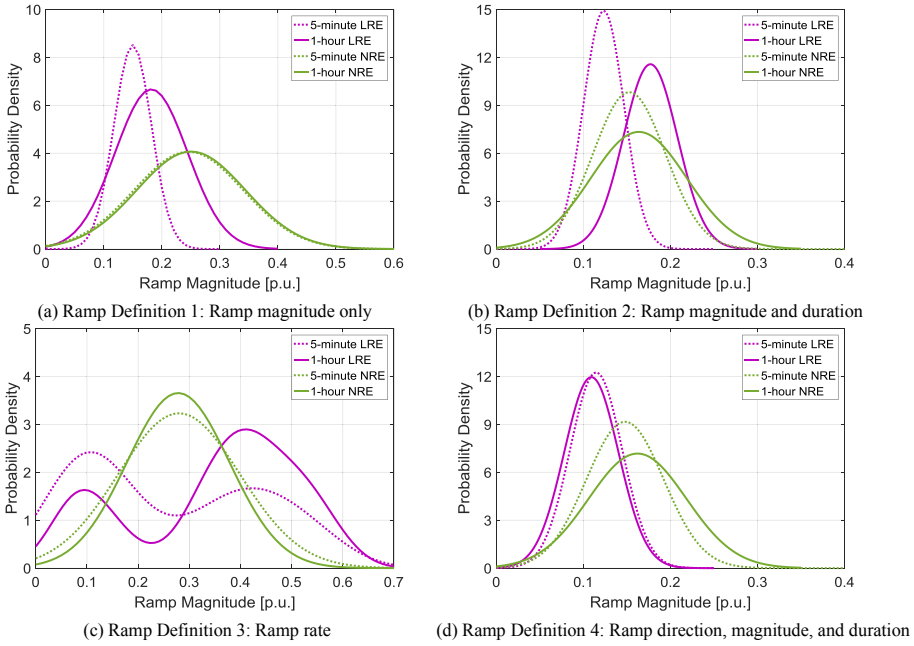

(a) Ramp Definition 1: Ramp magnitude only

(b) Ramp Definition 2: Ramp magnitude and duration

(c) Ramp Definition 3: Ramp rate

(d) Ramp Definition 4: Ramp direction, magnitude, and duration

Fig. 14. Comparison of ramping magnitude in load and netload.

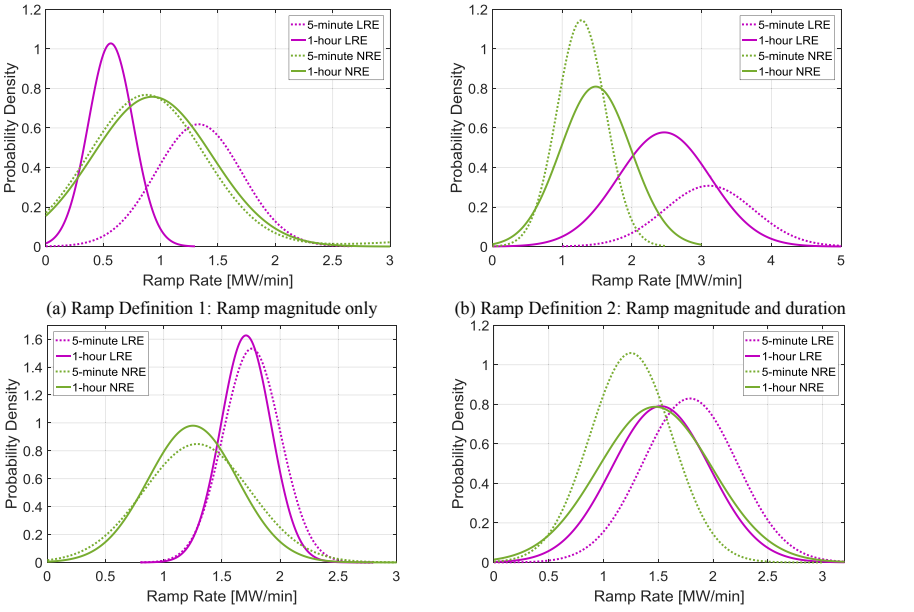

(a) Ramp Definition 1: Ramp magnitude only

(b) Ramp Definition 2: Ramp magnitude and duration

(c) Ramp Definition 3: Ramp rate

(d) Ramp Definition 4: Ramp direction, magnitude, and duration

Fig. 15. Comparison of ramping rate in load and netload.

similar with that of SPREs. Power system operators need to provide ramping reserves for the same period length to cope with both WPREs and SPREs in the UC model (at the 60-min time resolution).

5.4.2. Comparison of ramping magnitude

Fig. 17 compares the probability density distributions of ramping magnitude in wind power and solar power. For WPREs in Definition 1, the probability density of the ramping magnitude is lower with a smaller peak value and heavier tails from the 5-min time resolution to the 60-min time resolution. For WPREs in Definitions 1 to 4, the peak ramping magnitude values are approximately the same. Power system operators need to provide the same amount of ramping reserves to cope with WPREs in both the ED (at the 5-min time resolution) and the UC (at the 60-min time resolution) models.

For SPREs in Definitions 1 to 4, the peak ramping magnitude values at the 60-min time resolution are substantially larger than those at the 5-min time resolution. Power system operators need to provide substantially more ramping reserves to cope with SPREs in the UC model (at the 60-min time resolution) than in the ED model (at the 5-min time resolution).

At the 5-min time resolution (dash lines), the peak ramping magnitude values are approximately the same for both WPREs and SPREs. Power system operators need to provide the same amount of

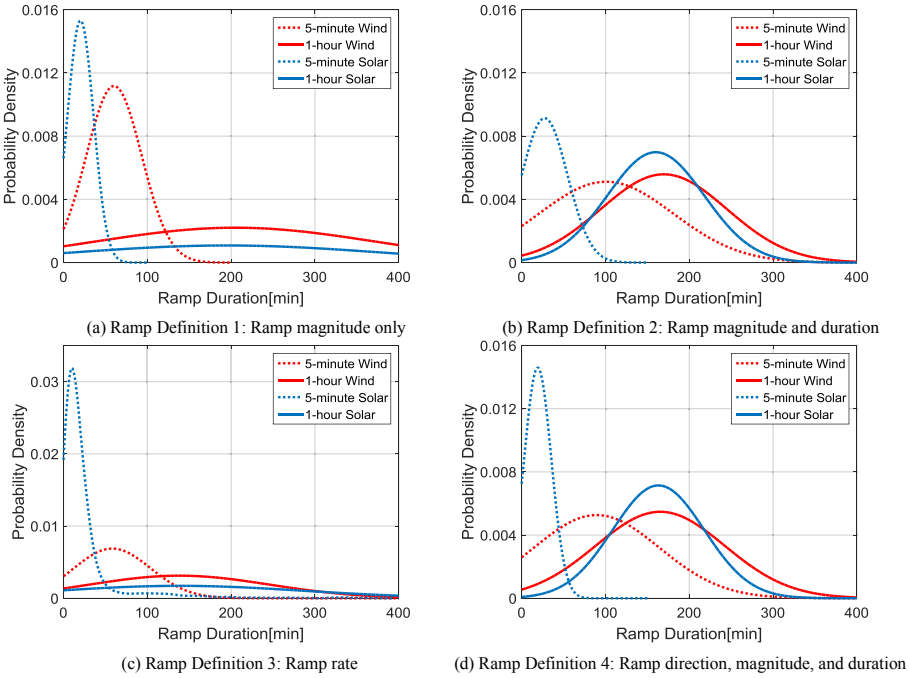

(a) Ramp Definition 1: Ramp magnitude only

(b) Ramp Definition 2: Ramp magnitude and duration

(c) Ramp Definition 3: Ramp rate

(d) Ramp Definition 4: Ramp direction, magnitude, and duration

Fig. 16. Comparison of ramping duration in wind power and solar power.

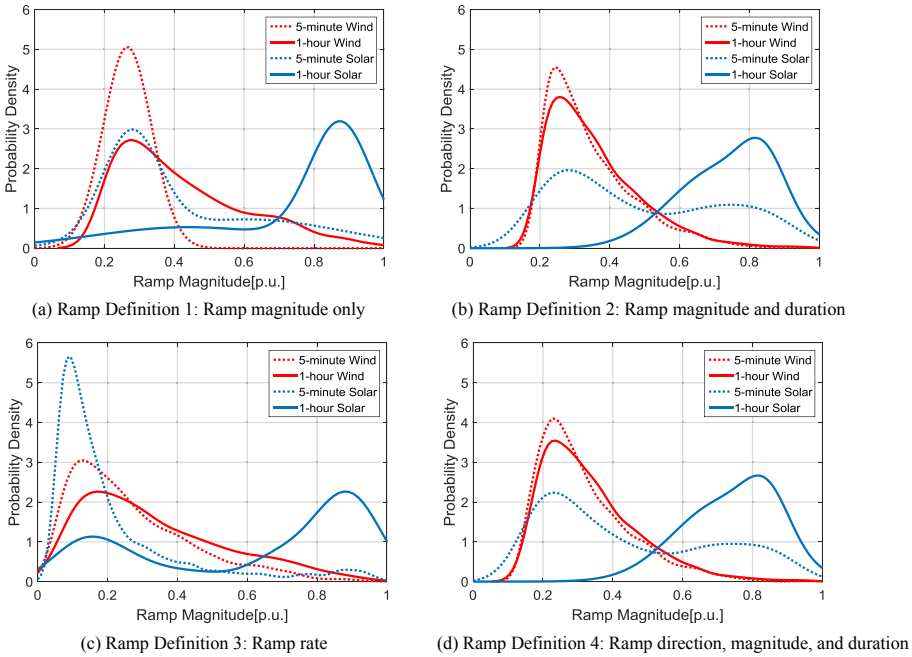

(a) Ramp Definition 1: Ramp magnitude only

(b) Ramp Definition 2: Ramp magnitude and duration

(c) Ramp Definition 3: Ramp rate

(d) Ramp Definition 4: Ramp direction, magnitude, and duration

Fig. 17. Comparison of ramping magnitude in wind power and solar power.

ramping reserves to cope with both WPREs and SPREs in the ED model (at the 5-min time resolution). At the 60-min time resolution (solid lines), the peak ramping magnitude values of SPREs are substantially larger than those of WPREs. Power system operators need to provide substantially more ramping reserves to cope with SPREs than to cope with WPREs in the UC model (at the 60-min time resolution).

5.4.3. Comparison of ramping rate

Fig. 18 compares the probability density distributions of ramping rate in wind power and solar power. For WPREs in Definitions 1, 2, and 4, the peak ramping rate values at the 5-min time resolution are larger than those at the 60-min time resolution. Power system operators need to prepare more fast generation to compensate for the high ramping rate of WPREs in the ED model (at the 5-min time resolution) than in the UC model (at the 60-min time resolution).

For SPREs in Definitions 1 to 4, the peak ramping rate values at the 5-min time resolution are larger than those at the 60-min time resolution. Power system operators need to prepare more fast

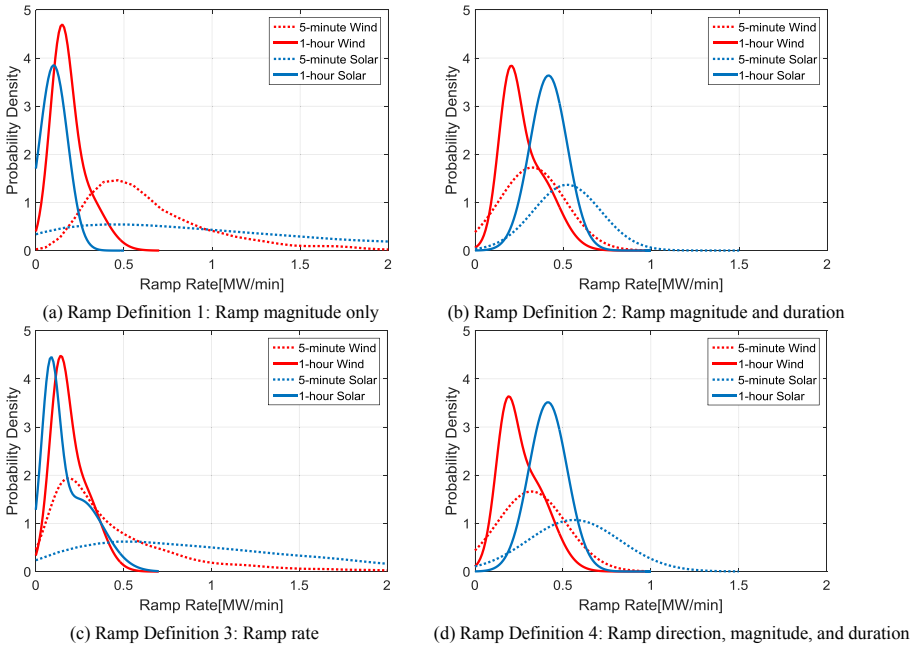

(a) Ramp Definition 1: Ramp magnitude only
(b) Ramp Definition 2: Ramp magnitude and duration
(c) Ramp Definition 3: Ramp rate
(d) Ramp Definition 4: Ramp direction, magnitude, and duration

Fig. 18. Comparison of ramping rate in wind power and solar power.

generation to compensate for the high ramping rate of SPREs in the ED model (at the 5-min time resolution) than in the UC model (at the 60-min time resolution).

At the 5-min time resolution (dash lines) in Definitions 2 to 4, the peak ramping rate values of SPREs are larger than those of WPREs. Power system operators need to prepare more fast generation to cope with SPREs than to cope with WPREs in the ED model (at the 5-min time resolution). At the 60-min time resolution (solid lines) in Definitions 1 and 3, the peak ramping values of WPREs are larger than those of SPREs. Power system operators need to prepare more fast generation to cope with WPREs than to cope with SPREs in the UC model (at the 60-min time resolution). At the 60-min time resolution in Definitions 2 and 4, the peak ramping values of SPREs are larger than those of WPREs. Power system operators need to prepare more fast generation to cope with SPREs than to cope with WPREs in the UC model (at the 60-min time resolution)."

6. Discussion and extension

Recent research has been widely performed on the statistical characterization of ramps by using the distribution models, such as the empirical distribution [14], Fréchet distribution (a generalized extreme value distribution) [53], and generalized Gaussian mixture model (GGMM) [54]. The distribution models of wind/solar ramping features (magnitude, duration, and rate) are adaptable to power system operations, such as using the ramping magnitude distribution model in the development of a new reserve product, and using the ramping duration and rate distribution models in the estimation of wind/solar power ramping rates.

6.1. Ramping magnitude

The probabilistic ramping magnitude could be applied to design new types of reserve products, such as the design of probabilistic wind power ramping product (WPRP). Taking the upward WPRP as an example based on the optimization model in Ref. [55], the ramping magnitude could be used to formulate the probabilistic constraints of upward flexible ramping reserve requirement and then deduced to be linear and deterministic by using the distribution model.

$$\begin{cases} \Pr\left\{\sum_{i=1}^{NI} fu_i + \sum_{j=1}^{NW} UP_j^{\mathrm{M}} \geqslant UR\right\} \geqslant c_{\mathrm{M}} \\ \Pr\left\{\sum_{i=1}^{NI} fu_i + \sum_{j=1}^{NW} UP_j^{\mathrm{M}} \geqslant UR\right\} \\ = 1 - \Pr\left\{UR - \sum_{i=1}^{NI} fu_i \geqslant \sum_{j=1}^{NW} UP_j^{\mathrm{M}}\right\} \\ = 1 - F_{\mathrm{M}}\left(UR - \sum_{i=1}^{NI} fu_i\right) \end{cases} \tag{26}$$

$$\Rightarrow UR - \sum_{i=1}^{NI} fu_i \leqslant F_{\mathrm{M}}^{-1}(1 - c_{\mathrm{M}}) \tag{27}$$

where fu_i is the scheduled flexible up-ramping reserve of conventional generator i. UP_j^{M} is the up-WPRP provided by the ramping magnitude of wind generator (or wind farm) j. UR is the total flexible up-ramping reserve requirement of the system. F_{M}^{-1} is the inverse function of the cumulative distribution function, F_{M}, of ramping magnitude. c_{M} is the confidence level which the probability of the ramping magnitude constraint should be greater than.

6.2. Ramping duration and rate

Power system operators need to decide at what rates ($\overline{R}$) the WPRs should be limited during operations. The distributions of ramping duration and rate could be used in power system optimization models (such as the model proposed in Ref. [14]) in an analytical manner. Given a ramp with random variables of ramping duration D and rate R, the compensation price ρ_1 (MW/hour) of the curtailed wind power when ramping rate is greater than the rate limit R, and the cost price ρ_2 (MW/hour) of fast generators to compensate a WPR with the rate limit $\overline{R}$, the total cost compensated to the wind plant is $\rho_1(R-\overline{R})D^2$ and the total cost of fast generators

is $\rho_2(\overline{R}-R)D^2$. The optimization model is to determine an optimal R that minimizes the total expected cost, given by:

$$\min E\left[\rho_1(R-\overline{R})_+D^2+\rho_2(\overline{R}-R)_+D^2\right] \tag{28}$$

This problem can be solved by using the distribution models of D and R. Assuming that the random variables R and D^2 are independent, this problem is deduced as:

$$\min(\rho_1-\rho_2)E[R]E\left[D^2\right]+(\rho_2-\rho_1)\overline{R}E\left[D^2\right] \tag{29}$$

where the expect value of R is $E[\mathrm{R}]=\int_{-\infty}^{+\infty}xf_{\mathrm{R}}(x)\mathrm{d}x$ and f_{R} is the probability distribution function of ramping rate. The expect value of D^2 is $E[D^2]=\int_{-\infty}^{+\infty}y^2f_{\mathrm{D}}(y)\mathrm{d}y$ and f_{D} is the probability distribution function of ramping duration.

7. Conclusion

This paper developed three ramping detection methods for wind power, solar power, load, and netload based on an optimized swinging door algorithm, and performed an extensive comparison of LREs and NREs at different renewable penetration levels. The three methods used swinging door algorithm as the first stage for segregating consecutive segments. The differences of the three methods mainly present in the second stage with a dynamic programming, which were: (i) for LREs and NREs detection, the dynamic programming was directly used to combine adjacent load or netload segments that were in the same ramping direction; (ii) for SPREs detection, ramp events occurring in both clear-sky and measured solar power were removed, after combining adjacent solar power segments by dynamic programming; and (iii) for WPREs detection, a process of merging "bumps" (that had a different changing direction) into adjacent ramping segments was included to improve the performance of dynamic programming. A metric was developed to evaluate the performance of ramp detection. This metric mainly focused on the detection accuracy of ramping starts and ramping ends, which were considered as the most important ramping features for power system operators. The metric evaluation results were visualized in a performance diagram in conjunction with a contingency table.

The ramping distribution moved closer to the x-axis when the penetration level increased. There were more ramps with shorter durations and smaller magnitudes occurring at the high renewable penetration. Moreover, the number of ramping events also increased with increasing the renewable penetration level. This observation would benefit power system operators in many ways, such as utilizing the ramping events information (e.g., ramping product market design) in system operations, or mitigate ramping events (e.g., ramping control based on energy storage system) for the power balance.

Results also showed that even with a low penetration of the renewable, the ramping characteristics were substantially different between load and netload. Ramping features are more stable in LREs than in NREs especially at the 1-h time resolution. It means the renewable penetration will definitely bring more ramping flexibility to its application, especially in the market design of ramping products. Should these increasing ramping characteristics be effectively taken into account, more potential revenue could be obtained for both wind power producers and system operators in the future electricity market.

Ramp events in wind, solar, load, and netload were characterized and analyzed for a utility in the northwestern United States. Accuracy estimation results showed that: (i) SPREs were more accurately detected than WPREs and NREs at both 5- and 15-min time resolutions; (ii) WPREs detection accuracy increased with the time resolution, and the 1-h time resolution had the best ramping detection performance; and (iii) NRE ramping features are more consistent among different time resolutions than WPREs and SPREs.

Future work will (i) study how to effectively and specifically use the ramping information of wind, solar, load, and netload in power system operations and electricity markets; and (ii) quantitatively evaluate the economic impacts of renewable energy on load and netload ramping events with different renewable penetrations.

Acknowledgements

This work was supported by the National Renewable Energy Laboratory under Subcontract No. XGJ-6-62183-01 (under the U.S. Department of Energy Prime Contract No. DE-AC36-08GO28308). This work was also supported by the National Basic Research Program of China (2012CB215101).

References

[1] P.S. Moura, A.T. Almeida, The role of demand-side management in the grid integration of wind power, Appl. Energy 87 (2010) 2581–2588.
[2] H. Jiang, Y. Zhang, J.J. Zhang, D.W. Gao, E. Muljadi, Synchrophasor-based auxiliary controller to enhance the voltage stability of a distribution system with high renewable energy penetration, IEEE Trans. Smart Grid (2015) 1–10.
[3] R. Dominguez, L. Baringo, A.J. Conejo, Optimal offering strategy for a concentrating solar power plant, Appl. Energy 98 (2012) 316–325.
[4] C.D. Jonghe, E. Delarue, R. Belmans, W. D'haeseleer, Determining optimal electricity technology mix with high level of wind power penetration, Appl. Energy 88 (2011) 2231–2238.
[5] J. Wang, A. Botterud, R. Bessa, H. Keko, L. Carvalho, D. Issicaba, J. Sumaili, V. Miranda, Wind power forecasting uncertainty and unit commitment, Appl. Energy 88 (2011) 4014–4023.
[6] Freedman J, Markus M, Penc R. Analysis of west Texas wind plant ramp-up and ramp-down events. [Online]. Available: http://interchange.puc.state.tx.us/WebApp/Interchange/Documents/33672_1014_580034.pdf.
[7] T. Godfrey, S. Mullen, R.C. Dugan, C. Rodine, D.W. Griffith, N. Golmie, Modeling smart grid applications with co-simulation, in: 1st IEEE International Conference on Smart Grid Communications, Gaithersburg, MD, 2010.
[8] NBC News: http://www.nbcnews.com/business/energy/britains-electric-grid-girds-world-cup-tea-surge-n118491.
[9] H. Wu, M. Shahidepour, A. Alabdulwahab, A. Abusorrah, Thermal generation flexibility with ramping costs and hourly demand response in stochastic security-constrained scheduling of variable energy sources, IEEE Trans. Power Syst. (2015) 1–10.
[10] L. Xu, D. Tretheway, Flexible Ramping Products, CAISO, 2012.
[11] N. Navid, G. Rosenwald, Market solutions for managing ramp flexibility with high penetration of renewable resource, IEEE Trans. Sustain. Energy 3 (4) (2012) 784–790.
[12] B. Wang, B.F. Hobbs, A flexible ramping product: can it help real-time dispatch markets approach the stochastic dispatch ideal? Electr. Power Syst. Res. 109 (2014) 128–140.
[13] E. Ela, B. Kirby, N. Navid, J.C. Smith, Effective ancillary services market designs on high wind power penetration systems, in: IEEE Power and Energy Society General Meeting, San Diego CA, 2012.
[14] R. Sevlian, R. Rajagopal, Detection and statistics of wind power ramps, IEEE Trans. Power Syst. 28 (4) (2013) 3610–3620.
[15] R. Sevlian, R. Rajagopal, Wind power ramps: detection and statistics, in: IEEE Power Energy Society Generation Meeting, San Diego, CA, 2012.
[16] J. Zhang, A.R. Florita, B.M. Hodge, J. Freedman, Ramp forecasting performance from improved short-term wind power forecasting, in: ASME International Design Engineering Technical Conference & Computers and Information in Engineering Conference (IDETC/CIE 2014), Buffalo, NY, 2014.
[17] M. Cui, J. Zhang, A.R. Florita, B.M. Hodge, D. Ke, Y. Sun, An optimized swinging door algorithm for identifying wind ramping events, IEEE Trans. Sustain. Energy 7 (1) (2016) 150–162.
[18] C. Kamath, Understanding wind ramp events through analysis of historical data, in: Proceedings Transmission and Distribution Conference Exposition, 2010.
[19] C. Kamath, Associating weather conditions with ramp events in wind power generation, in: Proceedings Transmission and Distribution Conference Exposition, 2011.
[20] M. Cui, D. Ke, Y. Sun, D. Gan, J. Zhang, B.M. Hodge, Wind power ramp event forecasting using a stochastic scenario generation method, IEEE Trans. Sustain. Energy 6 (2) (2015) 422–433.

[21] M. Cui, D. Ke, Y. Sun, D. Gan, J. Zhang, B.M. Hodge, A scenario generation method for wind power ramp events forecasting, in: IEEE Power and Energy Society General Meeting, Denver, CO, 2015.
[22] N. Cutler, M. Kay, K. Jacka, T.S. Nielsen, Detecting categorizing and forecasting large ramps in wind farm power output using meteorological observations and WPPT, Wind Energy 10 (5) (2007) 453–470.
[23] H. Zareipour, D. Huang, W. Rosehart, Wind power ramp events classification and forecasting: a data mining approach, in: IEEE Power Energy Society Generation Meeting, San Diego, CA, 2011.
[24] B. Greaves, J. Collins, J. Parkes, A. Tindal, Temporal forecast uncertainty for ramp events, Wind Eng. 33 (4) (2009) 309–320.
[25] M.L. Kubik, P.J. Coker, J.F. Barlow, Increasing thermal plant flexibility in a high renewables power system, Appl. Energy 154 (2015) 102–111.
[26] K. Porter, D. Yen-Nakafuji, B. Morgenstern, A review of the international experience with integrating wind energy generation, Electr. J. 20 (8) (2007) 48–59.
[27] Y. Chu, H. Pedro, M. Li, C. Coimbra, Real-time forecasting of solar irradiance ramps with smart image processing, Sol. Energy 114 (2015) 91–104.
[28] C.W. Hansen, J.S. Stein, A. Ellis, Statistical Criteria for Characterizing Irradiance Time Series, Tech. Rep. SAND 2010-7314, Sandia National Laboratories, Albuquerque, NM, 2010.
[29] Reno MJ, Stein JS. Using cloud classification to model solar variability. [Online]. Available: http://proceedings.ases.org/wp-content/uploads/2014/02/SOLAR2013_0190_final-paper.pdf.
[30] Willy DM, Dyreson A, Acker TL, Morgan E, Flood RK. [Online]. Available: http://nau.edu/CEFNS/Engineering/Mechanical/Researc-h-and-Labs/Energy/_Forms/Dead-Band-Ramp-Detection-ASES-2014-Final/.
[31] C.A. Hill, M.C. Such, D. Chen, J. Gonzalez, W.M. Grady, Battery energy storage for enabling integration of distributed solar power generation, IEEE Trans. Smart Grid 3 (2) (2012) 850–857.
[32] E. Arias-Castro, J. Kleissl, M. Lave, A poisson model for anisotropic solar ramp rate correlations, Sol. energy 101 (2014) 192–202.
[33] M. Hummon, J. Cochran, A. Weekley, A. Lopez, J. Zhang, B. Stoltenberg, B. Parsons, P. Batra, B. Mehta, D. Patel, Variability of Photovoltaic Power in the State of Gujarat Using High Resolution Solar Data, Tech. Rep. NREL/TP-7A40–60991, National Renewable Energy Laboratory, Golden, CO, 2014.
[34] B.M. Hodge, M. Hummon, K. Orwig, Solar ramping distributions over multiple timescales and weather patterns, in: 1st International Workshop on Integration of Solar Power into Power Systems, Aarhus, Denmark, 2011.
[35] A. Florita, B.M. Hodge, K. Orwig, Identifying wind and solar ramping events, in: IEEE 5th Green Technologies Conference, Denver, CO, 2013.
[36] M. Cui, J. Zhang, A. Florita, B.M. Hodge, D. Ke, Y. Sun, Solar power ramp events detection using an optimized swinging door algorithm, in: Proceedings of the ASME 2015 International Design Engineering Technical Conferences & Computers and Information in Engineering Conference, Boston, MA, 2015.
[37] H. Zheng, A. Kusiak, Prediction of wind farm power ramp rates: a data-mining approach, J. Sol. Energy Eng. 131 (3) (2009) 031011.
[38] C. Ferreira, J. Gama, L. Matias, A. Botterud, J. Wang, A Survey on Wind Power RAMP Forecasting, Tech. Rep. ANL/DIS-10-13, Argonne National Laboratory, DuPage County, IL, 2010.
[39] E.H. Bristol, Swinging door trending: adaptive trend recording?, in: Proceedings of ISA National Conference, 1990.
[40] Y.V. Makarov, C. Loutan, J. Ma, P. Mello, Operational impacts of wind generation on California Power Systems, IEEE Trans. Power Syst. 24 (2) (2009) 1039–1050.
[41] J. Ma, S. Lu, P.V. Etingov, Y.V. Makarov, Evaluating the impact of solar generation on balancing requirements in Southern Nevada System, in: IEEE Power Energy Society General Meeting, San Diego, CA, 2012.
[42] N.G. Boulaxis, M.P. Papadopoulos, Optimal feeder routing in distribution system planning using dynamic programming technique and GIS facilities, IEEE Trans. Power Deliv. 17 (1) (2002) 242–247.
[43] V. Marano, G. Rizzo, F.A. Tiano, Application of dynamic programming to the optimal management of a hybrid power plant with wind turbines, photovoltaic panels and compressed air energy storage, Appl. Energy 97 (2012) 849–859.
[44] C.W. Potter, E. Grimit, B. Nijssen, Potential benefits of a dedicated probabilistic rapid ramp event forecast tool, in: Proceedings of IEEE Power System Conference and Exposition (PSCE), Seattle, WA, 2009.
[45] L. Xu, D. Tretheway, Flexible Ramping Products, CAISO, 2012.
[46] Q. Wang, Y. Guan, J. Wang, A chance-constrained two-stage stochastic program for unit commitment with uncertain wind power output, IEEE Trans. Power Syst. 27 (1) (2012) 206–215.
[47] H. Wu, M. Shahidehpour, Z. Li, W. Tian, Chance-constrained day-ahead scheduling in stochastic power system operation, IEEE Trans. Power Syst. 29 (4) (2014) 1583–1591.
[48] P.J. Roebber, Visualizing multiple measures of forecast quality, Weather Forecast. 24 (2) (2009) 601–608.
[49] PV Performance Modeling Collaborative (PVPMC): https://pvpmc.sandia.gov/.
[50] C.B. Martinez-Anido, B. Botor, A.R. Florita, C. Draxl, S. Lu, H.F. Hamannn, B.M. Hodge, The value of day-ahead solar power forecasting improvement, Sol. Energy 129 (2016) 192–203.
[51] NREL: http://www.nrel.gov/electricity/transmission/wind_toolkit.html.
[52] MathWorks: http://www.mathworks.com/help/stats/ksdensity.html.
[53] D. Ganger, J. Zhang, V. Vittal, Statistical characterization of wind power ramps via extreme value analysis, IEEE Trans. Power Syst. 29 (6) (2014) 3118–3119.
[54] M. Cui, C. Feng, Z. Wang, J. Zhang, Q. Wang, A.R. Florita, V. Krishnan, B.M. Hodge, Probabilistic wind power ramp forecasting based on a scenario generation method, in: IEEE Power Energy Society General Meeting, Chicago, IL, 2017.
[55] M. Cui, J. Zhang, H. Wu, B.M. Hodge, Wind-friendly flexible ramping product design in multi-timescale power system operations, IEEE Trans. Sustain. Energy (2017), http://dx.doi.org/10.1109/tste.2017.2647781.